AIP | Applied Physics Letters

Temperature-dependent carrier–phonon coupling in topological insulator Bi2Se3

Yi-Ping Lai, Hsueh-Ju Chen, Kuang-Hsiung Wu, and Jia-Ming Liu

Citation: Applied Physics Letters **105**, 232110 (2014); doi: 10.1063/1.4904009
View online: http://dx.doi.org/10.1063/1.4904009
View Table of Contents: http://scitation.aip.org/content/aip/journal/apl/105/23?ver=pdfcov
Published by the AIP Publishing

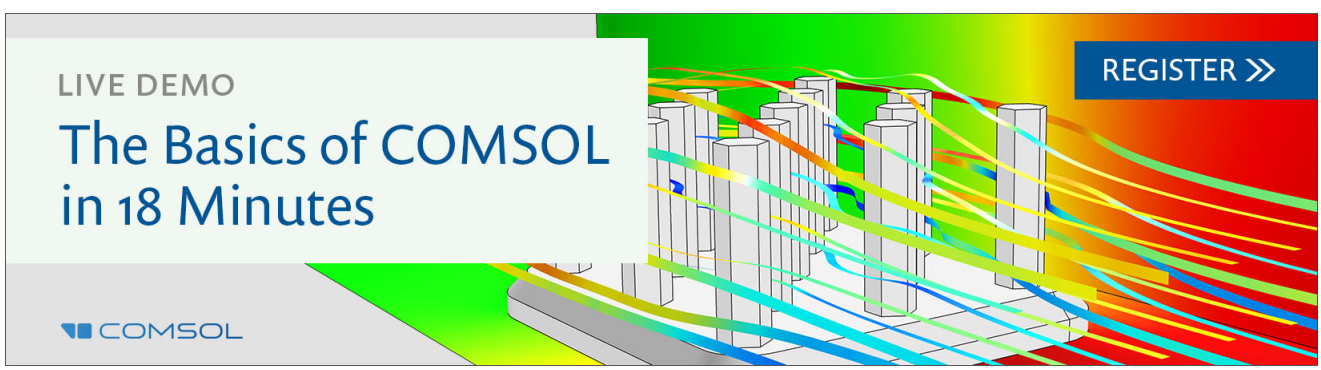

Temperature-dependent carrier–phonon coupling in topological insulator Bi_2Se_3

Yi-Ping Lai,[1] Hsueh-Ju Chen,[2] Kuang-Hsiung Wu,[2] and Jia-Ming Liu[1]
[1]*Electrical Engineering Department, University of California Los Angeles, Los Angeles, California 90095, USA*
[2]*Department of Electrophysics, National Chiao-Tung University, Hsinchu 300, Taiwan*

(Received 9 September 2014; accepted 26 November 2014; published online 9 December 2014)

Temperature-dependent (11.0 K−294.5 K) carrier–phonon coupling in Bi_2Se_3 is investigated by ultrafast pump−probe spectroscopy. The rise time of the differential reflectivity is interpreted by a combined effect of electron temperature relaxation and hot-phonon lifetime. The electron−phonon coupling constant of the bulk state ($\lambda = 0.63 \pm 0.05$) is deduced from theoretical fitting. Increasing hot-phonon lifetime with decreasing temperature is attributed to a decreasing phonon−phonon collision rate. A complete analysis of the thermalization process is presented. Understanding carrier and phonon dynamics is essential for future optoelectronic and spintronic applications of topological insulators. © *2014 AIP Publishing LLC*. [http://dx.doi.org/10.1063/1.4904009]

Topological insulators, such as Bi_2Se_3, Bi_2Te_3, and Sb_2Te_3, are a state of material, which shows an insulated bulk state and a conducting edge state protected by time-reversal symmetry. Time- and angle-resolved photoemission spectroscopy (trARPES)[1–4] and ultrafast pump−probe spectroscopy have been applied to study phonon and carrier dynamics in Bi_2Se_3.[5–9] Due to its high probe energy (∼6 eV), trARPES shows the dynamics at the surface, including complicated coupling between the bulk and surface states, which is difficult to disentangle. By contrast, the lower probe energy (∼1.5 eV) of ultrafast pump−probe spectroscopy enables it to examine the dynamics of the bulk state only. However, the differential reflectivity measured by pump−probe spectroscopy contains contributions of carriers and phonons. The interpretations of its rise and fall times were contradictory in the previous studies.[5–8]

In this paper, temperature-dependent pump−probe spectroscopy of Bi_2Se_3 is studied. According to the temperature dependency, the contributions of electrons and phonons are clarified by the two-temperature model (TTM) and the hot-phonon lifetime, respectively. The electron−phonon coupling constant ($\lambda = 0.63 \pm 0.05$) of the bulk state is obtained. A recent temperature-dependent study of $Bi_{1.5}Sb_{0.5}Te_{1.8}Se_{1.2}$[10] focused on the dynamics on a larger time scale in lightly doped materials, which is different from the purpose of this work.

For our experiment, *n*-type Bi_2Se_3 single crystals with a carrier concentration of 6×10^{19} cm^{-3} were synthesized by stoichiometric mixtures of 5N purity of Bi and Se in sealed, evacuated quartz tubes. The pump and probe pulses of 100 fs duration at a repetition rate of 5.1 MHz and a center wavelength of 800 nm were used. The fluences of the pump and probe pulses were 37 μJ/cm^2 and 2.5 μJ/cm^2, respectively. The polarizations of the pump and probe pulses were orthogonal to each other and both perpendicular to the surface normal of the sample. Liquid helium was used to continuously tune the temperature of the sample from 10 to 300 K with an accuracy of 0.5 K.

The temporal evolution of the differential reflectivity measured at an ambient temperature of 294.5 K is shown as the blue curve in Fig. 1. The resolution of the system was determined by the temporal cross-correlation of the pump and probe pulses, as shown by the black curve in Fig. 1. The pump and probe pulses completely overlapped at $t = 0$ ps.

The measured differential reflectivity includes signals on very different time scales. The characteristic times and the corresponding physical processes are listed in Table I. A constant residual differential reflectivity starting at $t < 0$ ps is related to residual carriers after carrier diffusion and recombination between successive pump pulses. In this study, we are not interested in these slow electron dynamics. The details of the temperature dependence for other dynamical processes are analyzed and presented below. The focus is on the dynamics of electron-phonon coupling during the first few picoseconds after the excitation.

The slow and fast oscillations can be attributed to coherent acoustic phonons and optical phonons, respectively. Coherent acoustic phonons oscillate at ∼0.04 THz; this oscillation quickly damps within 1–2 periods, as shown in Fig. 1. By contrast, coherent optical phonon oscillations, which are related to the A_{1g}^1 mode, last for tens of periods.

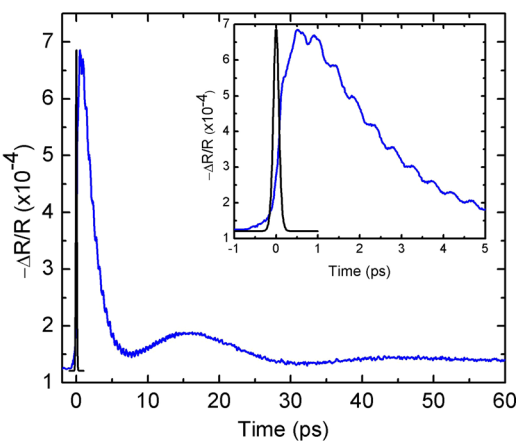

FIG. 1. Differential reflectivity measured at 294.5 K (blue). The temporal cross-correlation of the pump and probe pulses (black) is shown as a reference. The inset presents the same data for the first few picoseconds.

TABLE I. Characteristic times of the differential reflectivity and the corresponding physical processes.

Signal	Time	Physical process
Constant residual	$>10^{-7}$ s	Slow electron dynamics
Slow oscillation	$\sim 10^{10}$ Hz[a]	Coherent acoustic phonon
Fast oscillation	$\sim 10^{12}$ Hz[a]	Coherent optical phonon
Non-oscillatory signal	$<10^{-11}$ s	Electrons and incoherent phonons

[a]Oscillatory signals are characterized by their oscillation frequencies.

A 2-THz high-pass filter was applied to extract the fast oscillations; the resulting data were fitted by $e^{-t/\tau_{\text{dephasing}}} \sin(2\pi ft + \varphi)$ after 1 ps, as shown in Fig. 2(a). The frequency f and the dephasing time $\tau_{\text{dephasing}}$ of the optical phonons obtained through this fitting process for different ambient temperatures are summarized in Figs. 2(b) and 2(c). When the temperature increases, both f and $\tau_{\text{dephasing}}$ decrease due to lattice anharmonicity.[11] The temperature dependency is generally consistent with the recent observation by Raman spectroscopy.[12] However, the phonon dephasing time found in our experiment is longer than that measured using Raman spectroscopy, especially at 11.0 K. The discrepancy may be attributed to different phonon distributions in the momentum space measured through pump−probe spectroscopy and Raman spectroscopy.

As shown in the inset of Fig. 1, there is a non-oscillatory signal in the first few picoseconds. Its rise time is clearly longer than, but on the same order of, the cross-correlation trace of the pump and probe pulses. Therefore, the rise time can neither be simply explained by the finite durations of the pump and probe pulses nor by treating the pump and probe pulses as delta functions. In order to discuss the non-oscillatory signal, the residual at $t < 0$ ps was subtracted, and a 2-THz low-pass filter was used. The signal, $\Delta R_{\text{non-osc}}(t)$, was fitted by the following formula:

$$\Delta R_{\text{non-osc}}(t) = [a\Delta T_e(t) + b\theta(t)e^{-t/\tau_{\text{hot}}} * I(t)] * I(t), \quad (1)$$

where the first term in the bracket represents the dynamics of electron temperature, $\Delta T_e(t)$, and the second term represents the decay of incoherent hot-phonons with a lifetime τ_{hot}, $\theta(t)$ is the unit step function, a and b are time-independent fitting constants, $*$ represents the convolution of the two functions, and $I(t)$ is the pump/probe intensity profile given by

$$I(t) = \frac{1.7627}{2\Delta t}\,\text{sech}^2\left[\frac{1.7627t}{\Delta t}\right], \quad (2)$$

where Δt is the 100 fs pulse duration. In Eq. (1), a is positive because of the band filling effect introduced by excited electrons,[13] and b is assumed to be negative. Opposite signs for electron and phonon contributions to the differential reflectivity were also observed in other semiconductors.[14] The data were fitted from $t = -1$ ps to $t = 5$ ps in order to minimize the effect of the slow oscillation.

We assume that within the 100 fs pump pulse duration the electrons and incoherent phonons were thermalized to establish an electron temperature T_e and a lattice temperature T_L, respectively, but it took a longer time for the equilibrium between the electron and lattice temperatures to be reached. This assumption is supported by experimental observations under similar pump conditions.[2–4] Therefore, we must use the TTM to simulate the relaxation of the electron temperature. The Bi_2Se_3 sample was highly n-type doped. Therefore, the pump pulse energy was mainly absorbed by the electrons in the bulk conduction band so that we can use the Debye model to describe the electron−phonon coupling.[15] The initial lattice and electron temperatures were equal to the ambient temperature, which was set at a fixed temperature that ranged from 11.0 K to 294.5 K in the experiment. The temporal evolutions and spatial distributions of the electron and lattice temperatures can be simulated by the following rate equations:

$$\gamma_e T_e \frac{d}{dt}T_e = \frac{(1-R)FI(t)e^{-z/d}}{d} - U_{e\text{-ph}}(T_e, T_L), \quad (3)$$

$$C_L \frac{d}{dt}T_L = -C_L D \frac{d^2}{dz^2}T_L + U_{e\text{-ph}}(T_e, T_L), \quad (4)$$

where γ_e is the electron specific heat coefficient, R is the reflectivity, F is the pump fluence, d is the absorption depth, C_L is the Debye phonon heat capacity, D is the thermal diffusion coefficient, and $U_{e\text{-ph}}$ is the electron−phonon energy coupling rate given by[15]

$$U_{e\text{-ph}}(T_e, T_L) = 4g_\infty \theta_D \left[\left(\frac{T_e}{\theta_D}\right)^5 \int_0^{\frac{\theta_D}{T_e}} \frac{x^4}{e^x - 1}dx - \left(\frac{T_L}{\theta_D}\right)^5 \int_0^{\frac{\theta_D}{T_L}} \frac{x^4}{e^x - 1}dx\right], \quad (5)$$

where g_∞ is the electron−phonon coupling coefficient, and θ_D is the Debye temperature. We ignore the spatial variations

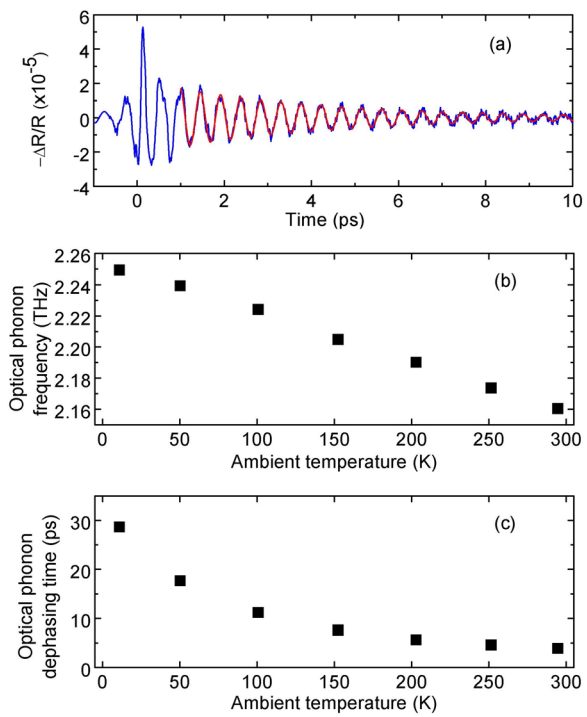

FIG. 2. (a) Coherent phonon oscillation extracted by a 2-THz high-pass filter (blue) fitted by a damped oscillation (red) after 1 ps at 294.5 K. (b) Coherent phonon frequencies and (c) dephasing times at different ambient temperatures.

TABLE II. Material parameters of Bi_2Se_3.

γ_e	$10\,J\,m^{-3}\,K^{-2}$	Reference 2
C_L	$2.81\times10^{19}k\left(\frac{T_L}{\theta_D}\right)^3\int_0^{\theta_D/T_L}\frac{x^4e^x}{(e^x-1)^2}dx$	Reference 20
θ_D	180 K	Reference 21
D	$0.3\times10^{-4}\,m^2\,s^{-1}$	Reference 22
R	0.5	Reference 23
d	$2.6\times10^{-8}\,m$	Reference 23

in the x and y directions parallel to the sample surface because the laser spot size (35 μm) is much larger than the absorption depth (26 nm). Except for g_∞, which is the only fitting parameter, all other physical parameters are experimentally measured values reported in the literature.[2,16–19] The values of these physical parameters are listed in Table II.

Represented by the first term in Eq. (1), the electron contribution to the differential reflectivity is proportional to the convolution of the temporal profile of the probe pulse intensity and that of the electron temperature variation on the surface, $\Delta T_e(t) * I(t)$. In Fig. 3, the best fitting of the simulation results obtained with $g_\infty = 1.4\times10^{16}\,J\,K^{-1}\,s^{-1}\,m^{-3}$ are compared to the experimentally measured electron dynamics for different ambient temperatures, which are obtained by subtracting the incoherent hot-phonon effect represented by the second term of Eq. (1) from the non-oscillatory differential reflectivity signal. The relaxation time scale of $\Delta T_e(t) * I(t)$ found from the simulation is consistent with the experimental data. For an ambient temperature between 294.5 K and 100.0 K, both experimentally measured and theoretically simulated temporal profiles of $\Delta T_e(t) * I(t)$ decay slightly faster at a lower ambient temperature. However, the experimentally measured decay abruptly slows down at 50.5 K and 11.0 K, but the theoretically simulated decay slows down slightly only at 11.0 K. Despite our best effort in getting the best fit by finely varying the electron−phonon coupling coefficient, we were not able to remove this inconsistency. This implies that the current model is not fully applicable when the ambient temperature is lower than 100.0 K. A close examination of the experimentally measured traces for 50.5 K and 11.0 K in Fig. 3 reveals that each of these two traces shows two different decay rates: a lower rate within several hundred femtoseconds after excitation and a higher rate afterwards. A comparison of these two traces clearly indicates that this phenomenon is more significant for 11.0 K than for 50.5 K. By contrast, this phenomenon is not observable in the experimental traces measured at higher temperatures. One possible explanation is that as the electrons dump energy to the lattice, the phonon−phonon collisions at a temperature below 100.0 K are too slow for the phonons to instantaneously reach thermal equilibrium, leading to nonequilibrium hot-phonons. Hot-phonons can effectively lower the rate of electron energy loss,[22,23] thus slowing down the decay of the experimental traces measured at 50.5 K and 11.0 K. As the phonons reach equilibrium after several hundred femtoseconds, the decay of these experimental traces accelerates. It should be noted, however, that the deviation at the low ambient temperatures may also result from the fitting error of the second term in Eq. (1).

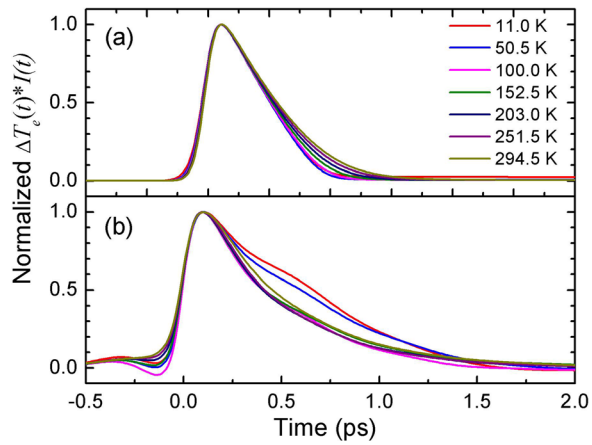

FIG. 3. (a) Theoretically simulated and (b) experimentally measured relaxations of the electron temperature at different ambient temperatures. The data were normalized by its peak values.

When $T_e, T_L > \theta_D$, the energy transfer between electrons and phonons has a particularly simple form. In this case, g_∞ can be directly related to the dimensionless electron−phonon coupling constant λ (Ref. 20)

$$U_{e\text{-}ph}(T_e,T_L) \simeq g_\infty(T_e - T_L) = \frac{3\hbar\lambda\gamma_e\langle\omega^2\rangle}{\pi k}(T_e - T_L), \quad (6)$$

where $\hbar$ is the reduced Plank constant, k is the Boltzmann constant, and $\langle\omega^2\rangle$ is the mean square phonon frequency, which can be calculated by the Debye spectrum of phonons with θ_D. Based on the parameters we used and listed in Table II, the dimensionless electron−phonon coupling constant is found to be $\lambda = 0.57\pm0.05$, which is larger than that of the Bi_2Se_3 surface state ($\lambda = 0.08 \sim 0.43$[21–23]). This large λ value suggests that the measured differential reflectivity is dominated by the bulk state, including strong electron−polar-phonon coupling.[5,24]

Incoherent phonon dynamics can be examined by studying the fitting time constant τ_{hot} in Eq. (1). The second term in Eq. (1) mainly determines the decay of the differential reflectivity for the first few picoseconds. The time constant τ_{hot} is related to the incoherent phonons emitted by electrons during the relaxation process. In the analysis presented above, we assume that the electrons couple to all phonon modes at the same rate and the phonons are thermalized instantaneously. However, excited electrons emit acoustic, optical, and polar-optical phonons via different mechanisms at different rates such as deformation potential, piezoelectric fields, and Fröhlich interaction. The coupling to the polar-optical phonons by Fröhlich interaction is expected to be stronger than the other electron−phonon coupling mechanisms.[24] Energy may accumulate in strongly coupled phonon modes and then gradually decay into lower-energy phonon modes with an effective time constant τ_{hot}. As shown in Fig. 4, τ_{hot} increases when the ambient temperature decreases, which can be attributed to a smaller phonon−phonon collision rate at a lower temperature. The temperature dependence and the order of magnitude of the phonon lifetime are consistent with those found in the previous studies.[25,26] A long phonon lifetime at a low temperature further supports

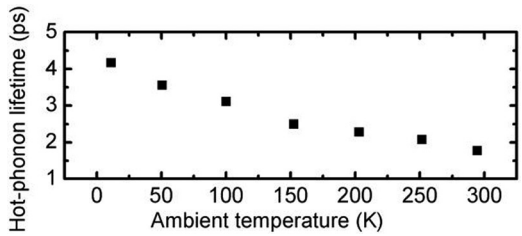

FIG. 4. Hot-phonon lifetime at different ambient temperatures.

the possibility stated in the preceding section that the TTM fails at low temperatures because of nonequilibrium hot-phonons.

In Fig. 5, the theoretically simulated temporal evolution of the differential reflectivity (red dashed curves) is compared to the experimentally measured non-oscillatory signal (blue dashed curves), where the data were normalized by the peak values of the experimentally measured non-oscillatory signal. Since the 2-THz low-pass filter applied to smooth out the coherent phonon oscillations also distorts the short rise time (blue solid and dashed curves), we further adjusted g_∞ to fit the original rise time of the normalized differential reflectivity from $t = -1$ ps to $t = 1$ ps. The best fitting, shown in red solid curves in Fig. 5, is obtained with $g_\infty = 1.5278 \times 10^{16}\ \mathrm{J\,K^{-1}\,s^{-1}\,m^{-3}}$, which corresponds to $\lambda = 0.63 \pm 0.05$. The fitting results are in good agreement with the experimental data. The deviation of the peak position at the two low temperatures of 50.5 K and 11.0 K results from the faster decay of the simulated $\Delta T_e(t) * I(t)$ compared to the experimental data, as seen in Fig. 3 and discussed above. Note that the small kink at $t = 0$ ps in the red fitting curve is an artifact caused by the use of the unit step function $\theta(t)$ in Eq. (1) for the hot-phonon term.

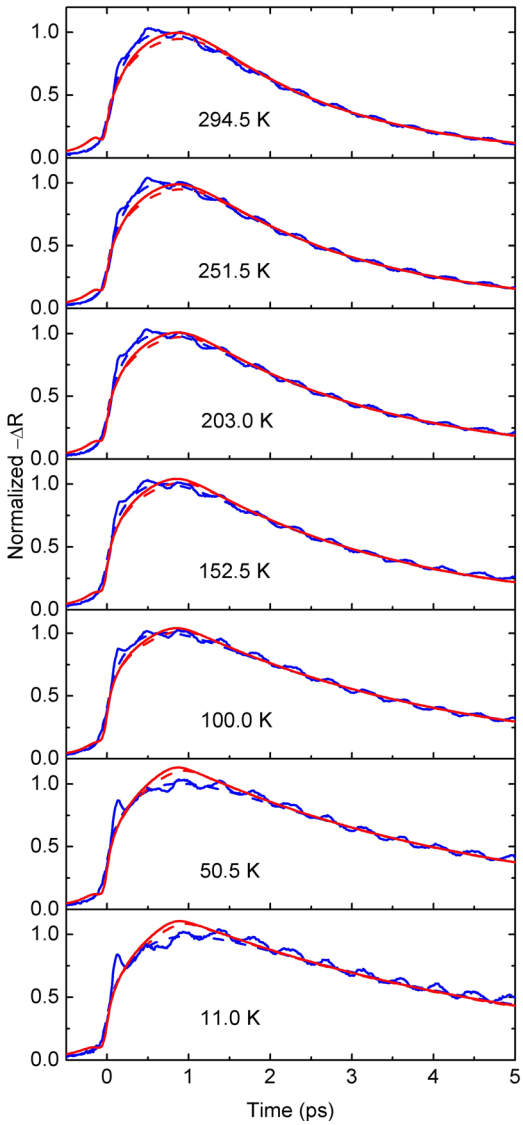

FIG. 5. Experimentally measured differential reflectivity (blue solid) and best fitting result (red solid) for different ambient temperatures. The non-oscillatory signal (blue dashed) and the corresponding theoretically fitting result (red dashed) are shown as references. The data were normalized by the peak values of the experimentally measured non-oscillatory signal. The small kink at $t = 0$ ps in each red fitting curve is an artifact caused by the use of the unit step function $\theta(t)$ in Eq. (1) for the hot-phonon term.

In summary, we have experimentally measured and theoretically analyzed the temperature-dependent carrier–phonon thermalization dynamics of Bi_2Se_3 through time-resolved differential reflectivity. A complete analysis is presented for the thermalization process by accounting various mechanisms, including electron−phonon coupling, hot-phonon effect, and coherent phonon oscillations. The electron−phonon coupling constant of the bulk state, $\lambda = 0.63 \pm 0.05$, is obtained in this study, implying that the measured signal was dominated by the dynamics of the bulk state. To better explain the experimental data at low ambient temperatures, the different electron−phonon coupling rates between different phonon modes have to be considered. Characterization of the electron−phonon coupling of the bulk state is important for understanding the interaction between the bulk and surface states on the surface, which is essential for future optoelectronic and spintronic applications of topological insulators.

This work was supported by U.S. Air Force AOARD under Grant Award No. FA2386-13-1-4022 and by Ministry of Science and Technology of Taiwan, R.O.C., under Grant No. NSC 102-2112-M-009-006-MY3.

[1]S. Sim, M. Brahlek, N. Koirala, S. Cha, S. Oh, and H. Choi, Phys. Rev. B **89**, 165137 (2014).
[2]Y. H. Wang, D. Hsieh, E. J. Sie, H. Steinberg, D. R. Gardner, Y. S. Lee, P. Jarillo-Herrero, and N. Gedik, Phys. Rev. Lett. **109**, 127401 (2012).
[3]J. A. Sobota, S. Yang, J. G. Analytis, Y. L. Chen, I. R. Fisher, P. S. Kirchmann, and Z. X. Shen, Phys. Rev. Lett. **108**, 117403 (2012).
[4]A. Crepaldi, B. Ressel, F. Cilento, M. Zacchigna, C. Grazioli, H. Berger, P. Bugnon, K. Kern, M. Grioni, and F. Parmigiani, Phys. Rev. B **86**, 205133 (2012).
[5]Y. D. Glinka, S. Babakiray, T. A. Johnson, A. D. Bristow, M. B. Holcomb, and D. Lederman, Appl. Phys. Lett. **103**, 151903 (2013).
[6]N. Kumar, B. A. Ruzicka, N. P. Butch, P. Syers, K. Kirshenbaum, J. Paglione, and H. Zhao, Phys. Rev. B **83**, 235306 (2011).
[7]D. Hsieh, F. Mahmood, J. W. McIver, D. R. Gardner, Y. S. Lee, and N. Gedik, Phys. Rev. Lett. **107**, 077401 (2011).
[8]J. Qi, X. Chen, W. Yu, P. Cadden-Zimansky, D. Smirnov, N. H. Tolk, I. Miotkowski, H. Cao, Y. P. Chen, Y. Wu, S. Qiao, and Z. Jiang, Appl. Phys. Lett. **97**, 182102 (2010).
[9]C. W. Luo, H. J. Wang, S. A. Ku, H. J. Chen, T. T. Yeh, J. Y. Lin, K. H. Wu, J. Y. Juang, B. L. Young, T. Kobayashi, C. M. Cheng, C. H. Chen, K. D. Tsuei, R. Sankar, F. C. Chou, K. A. Kokh, O. E. Tereshchenko, E. V. Chulkov, Y. M. Andreev, and G. D. Gu, Nano Lett. **13**, 5797 (2013).
[10]L. Cheng, C. La-o-Vorakiat, C. S. Tang, S. K. Nair, B. Xia, L. Wang, J. X. Zhu, and E. E. M. Chia, Appl. Phys. Lett. **104**, 211906 (2014).
[11]J. Menendez and M. Cardona, Phys. Rev. B **29**, 2051 (1984).

[12]B. Irfan, S. Sahoo, A. P. S. Gaur, M. Ahmadi, M. J. F. Guinel, R. S. Katiyar, and R. Chatterjee, J. Appl. Phys. **115**, 173506 (2014).
[13]S. S. Prabhu and A. S. Vengurlekar, J. Appl. Phys. **95**, 7803 (2004).
[14]A. Othonos, J. Appl. Phys. **83**, 1789 (1998).
[15]M. Kaganov, I. Lifshitz, and L. Tanatarov, Sov. Phys. JETP **4**(2), 173 (1957).
[16]C. Kittel, *Introduction to Solid State Physics* (Wiley, 1956).
[17]G. E. Shoemake, J. A. Rayne, and R. W. Ure, Phys. Rev. **185**, 1046 (1969).
[18]S. D. George, S. Augustine, E. Mathai, P. Radhakrishnan, V. P. N. Nampoori, and C. P. G. Vallabhan, Phys. Status Solidi A **196**, 384 (2003).
[19]J. W. McIver, D. Hsieh, S. G. Drapcho, D. H. Torchinsky, D. R. Gardner, Y. S. Lee, and N. Gedik, Phys. Rev. B **86**, 035327 (2012).
[20]P. B. Allen, Phys. Rev. Lett. **59**, 1460 (1987).
[21]X. T. Zhu, L. Santos, C. Howard, R. Sankar, F. C. Chou, C. Chamon, and M. El-Batanouny, Phys. Rev. Lett. **108**, 185501 (2012).
[22]Z. H. Pan, A. V. Fedorov, D. Gardner, Y. S. Lee, S. Chu, and T. Valla, Phys. Rev. Lett. **108**, 187001 (2012).
[23]R. C. Hatch, M. Bianchi, D. D. Guan, S. N. Bao, J. L. Mi, B. B. Iversen, L. Nilsson, L. Hornekaer, and P. Hofmann, Phys. Rev. B **83**, 241303(R) (2011).
[24]H. Ehrenreich, F. Seitz, and D. Turnbull, *Solid State Physics* (Elsevier Science, 1984).
[25]W. Richter and C. Becker, Phys. Status Solidi B **84**, 619 (1977).
[26]A. D. LaForge, A. Frenzel, B. C. Pursley, T. Lin, X. F. Liu, J. Shi, and D. N. Basov, Phys. Rev. B **81**, 125120 (2010).